

Near-field enhancement of infrared intensities for *f-f* transitions in Er³⁺ ions close to the surface of silicon nanoparticles

Lesya Borowska · Stephan Fritzsche · Pieter G. Kik · Artém E. Masunov

Received: 7 February 2010 / Accepted: 20 March 2010 / Published online: 20 May 2010
© Springer-Verlag 2010

Abstract Erbium doped waveguide amplifiers can be used in optical integrated circuits to compensate for signal losses. Such amplifiers use stimulated emission from the first excited state ($^4I_{13/2}$) to the ground state ($^4I_{15/2}$) of Er³⁺ at 1.53 μm, the standard wavelength for optical communication. Since the *intra-f* transitions are parity forbidden for free Er³⁺ ions, the absorption and the emission cross sections are quite small for such doped amplifiers. To enhance the absorption, Si nanoclusters can be embedded in silica matrix. Here we investigate the effect of the Si nanocluster on the Er³⁺ emission using *ab initio* theory for the first time. We combine multi-reference configuration interaction with one-electron spin-orbit Hamiltonian and relativistic effective core potentials. Our calculations show that the presence of a polarizable Be atom at 5 Å from the Er³⁺ ion in a crystalline environment can lead to an enhancement in the emission by a factor of three. The

implications of this effect in designing more efficient optical gain materials are discussed.

Keywords *Ab initio* theory · Erbium doped waveguide amplifiers · Optical gain materials · Spin-orbit coupling

Introduction

During the last decade, experiments with Er³⁺ doped in different solids have stimulated considerable effort in many areas of basic and applied research, including optical waveguides [1], thermometric measurements [2], and lasing [3]. In fiber-optic technology, for instance, the use of erbium-doped silica based glasses have found increasing use for signal amplification [4]. In these materials, the transitions between the electronic states of Er³⁺ in solids remain very similar to the ones of the free ion due to the tight localization of *f*-electrons near to the ionic core. For Er³⁺ in the gas phase *f-f* transitions are dipole forbidden, while certain atomic environments and the thermal motion may break the symmetry and make these transitions weakly allowed. As a result, Er ions if embedded into a solid can be excited into the metastable $^4I_{13/2}$ state (either through direct excitation into the higher lying $^4I_{11/2}$ state followed by relaxation, or by other means) and amplify the passing light pulse by stimulated emission. The resonant wavelengths of the $^4I_{13/2}$ to $^4I_{15/2}$ transitions in Er³⁺ fall into so called “telecommunication window”, the interval of maximum transparency of silica based glasses as applied in fiber-optics.

To increase the absorption probability and to eliminate the need in expensive pump lasers of a specific frequency, glasses can be co-doped with Si nanoclusters by plasma-enhanced chemical vapor deposition [5] or ion implantation [6]. The excitation energy is then transferred to the Er³⁺ cations with similar to 60% efficiency [7]. Such doping with

L. Borowska · A. E. Masunov (✉)
NanoScience Technology Center, Department of Chemistry,
and Department of Physics, University of Central Florida,
Orlando, FL 32826, USA
e-mail: amasunov@mail.ucf.edu

P. G. Kik
CREOL, The College of Optics and Photonics,
University of Central Florida,
Orlando, FL 32816, USA

L. Borowska
Institute for Nuclear Research NAS of Ukraine,
03680 Kyiv, Ukraine

L. Borowska
University of Bonn,
53121 Bonn, Germany

S. Fritzsche
Gesellschaft für Schwerionenforschung (GSI),
64291 Darmstadt, Germany

Si nanoclusters was shown to increase the overall Er^{3+} absorption cross-section by 3 orders of magnitude [8]. Extended x-ray absorption fine structure spectroscopy measurements indicate, moreover, that no direct interaction between Er and Si occurs [5], and that the environment of Er in Si doped glasses is similar to that of type C sesquioxide Er_2O_3 . Since Er_2O_3 and Y_2O_3 have the same crystal structure with nearly the same lattice constant, doping Y_2O_3 with Er^{3+} allows to introduce a controlled concentration of Erbium into the highly ordered crystalline environment. These doped crystals hold promise of first-rate laser host material [8] and may serve as a model for Er in silica glasses.

Some experimental findings [9–11] have shown another effect of Si nanoclusters if co-doped with Er^{3+} in silica glasses: namely, the pronounced increase of the direct $^4I_{13/2}$ to $^4I_{15/2}$ transition probabilities. Although an alternative interpretation of these observations do exist [12, 13], a direct proof is complicated due to various experimental factors. The goal of this study is to analyze and evaluate the possibility and magnitude of this enhancement from first principles.

From the viewpoint of classical electrodynamics, this enhancement effect can be given the following explanation. The homogeneous electric field of the incident light is perturbed within the proximity of the Si nanocluster with their higher dielectric constant than in the surrounding silica matrix. Assuming that the nanocluster can be approximated by a dielectric sphere, both the electric field and the field gradient are considerably distorted from their homogeneous values near to the poles of the sphere (Fig. 1). The enhanced field strength uniformly increases all the dipole transition probabilities of Er ion if they are placed near the poles of the nanocluster. In optics this is known as a near-field effect. From the viewpoint of quantum mechanics, the classical polarization has to be described in terms of the excited states of the unperturbed system, making different contributions to the ground and excited state of the perturbed system. Therefore, one needs to evaluate the contributions of the Si nanocluster into both ground and excited state wavefunctions of the combined system in order to evaluate the transition dipole moments. The effect of the polarizable nanocluster is hereby expected to be different for different transitions.

Obviously, a Si nanocluster is too large in order to be treated explicitly by quantum mechanics methods. Macroscopic theory suggests the enhancement of spontaneous emission for dipole transitions in the proximity of the nanoparticle [14]. However, these estimates were made under the conditions of a plasmon resonance and are not directly applicable to semi-conducting Si nanocrystals. Up to the present, no solid numerical estimates of this effect were made. Here we employ another approximation by replacing the nanocluster with a single polarizable atom and by extrapolating the results to the system of interest.

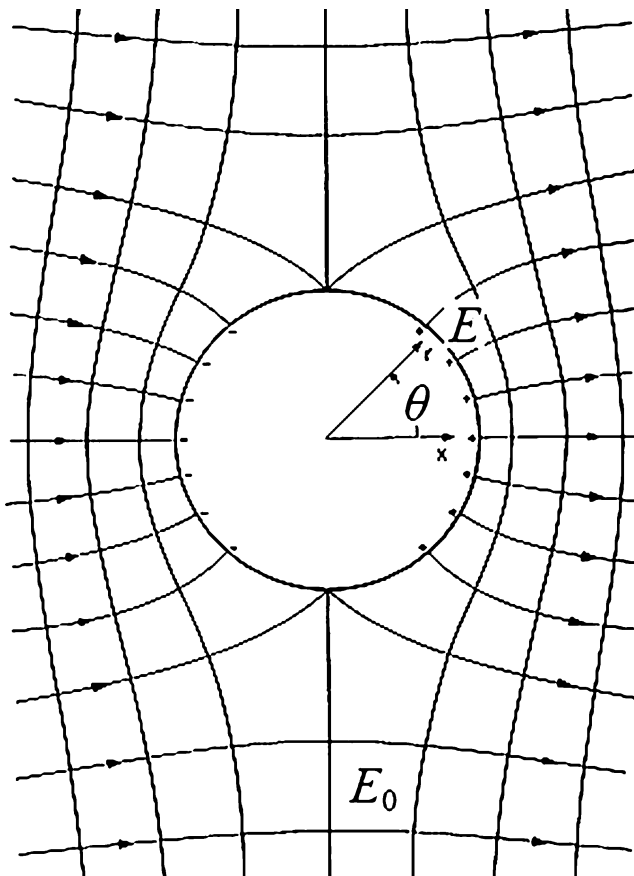


Fig. 1 Near-field effect in classical electrodynamics: the presence of polarizable sphere leads to a modification of the field strength and the field gradient immediately outside the sphere

Computational details

In atoms and ions of heavy elements, such as Er, relativistic effects cannot be neglected. As a result, the projections of the spin and orbital angular momenta are no longer well-defined quantum numbers by its own (as in the so-called intermediate *LS*-coupling) but have to be replaced by the total angular momentum and its projection. The phenomenological treatment of these spin-coupling effects is well developed and can be taken into account both for the crystal field and for the vibronic effects on electronic transitions in solids that contain *d*- and *f*-elements [15, 16]. However, this approach cannot account for the effect of some polarizable environment. Here we apply *ab initio* methods of electronic structure theory. The basic approach to spin-orbit coupling is based on the four component Dirac-Coulomb equation, which includes the spin-orbit operator implicitly. Molecular Dirac-Hartree-Fock programs have become increasingly available [17–19], and recent efforts have extended the four-component calculations of molecules and small clusters to include also electron-electron correlations [20, 21]. However, the spin-orbit coupling can be explicitly treated

C₂ site

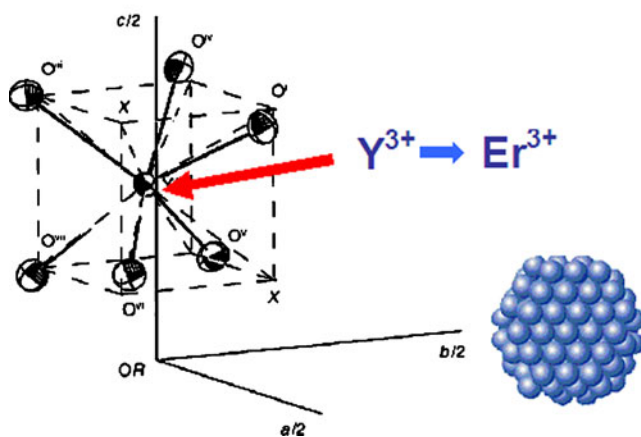


Fig. 2 Schematic representation of the system under study: An erbium atom replaces an yttrium atom at the C₂ site in the Y₂O₃ crystal structure. The nearby silicon nanocluster is modeled by the highly polarizable beryllium atom

within the single component quantum chemistry packages *via* the Breit-Pauli Hamiltonian [22]. Here we employed the GAMESS suite of programs [23] which implements spin-orbit configuration interaction (CI). This method uses LS-coupled CI eigenstates as the basis, evaluates the matrix elements for the Breit-Pauli operator and diagonalizes this Hamiltonian matrix in order to obtain spin-mixed wave functions. This method was shown to be accurate in

Table 1 The lowest energy levels of Er³⁺ calculated for systems I and II, compared to the experimentally measured values for C₂ site of the cubic Y₂O₃ crystal [8]

Energy (cm ⁻¹) (theory, I)	Energy (cm ⁻¹) (theory, II)	Energy (cm ⁻¹) (experiment)
⁴ I _{15/2}		
0	0	0
60	31	36
100	80	77
129	140	90
172	182	163
255	269	258
449	448	492
486	502	507
⁴ I _{13/2}		
6505	6506	6510
6562	6537	6548
6594	6590	6583
6638	6644	6602
6714	6722	6690
6863	6864	6835
6919	6940	6861

predicting the fine structure splitting for the low-lying atomic terms for the transition elements [23, 24] and the lanthanides [19]. Following Ref. [24], we have been using the SBKJC effective core potentials (ECPs) and basis sets, proposed by Stevens et al. [25]. To account for the polarization of the *f*-electrons by the crystalline environment, the SBKJC basis was augmented with four Gaussian primitive functions, contracted into one *g*-function according to Cao and Dolg [26]. The advantage of using relativistic ECP is that the valence orbitals are adjusted for spin-free relativistic orbital contractions and expansions. In order to account for the spin-orbit effect of the [Xe] core electrons, implicitly treated by means of the ECP, the nuclear charge in the one-electron part of Breit-Pauli Hamiltonian was adjusted

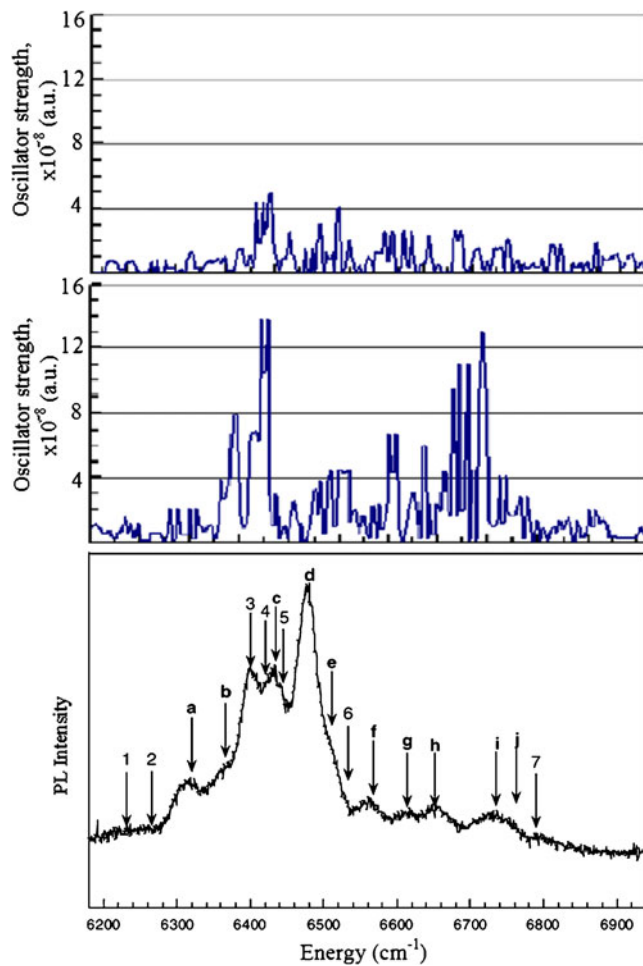


Fig. 3 Infrared emission spectrum of Er³⁺ doped Y₂O₃ for the ⁴I_{13/2}→⁴I_{15/2} transitions (at the C₂ symmetry sites). (Top panel) Model system I: Polarizable Be atom is 50 Å from ion Er³⁺; (Middle panel) Model system II: Polarizable Be atom is 5 Å from Er³⁺ ion; (Bottom panel) Experimental infrared emission spectrum of Er³⁺ doped Y₂O₃ for the ⁴I_{13/2}→⁴I_{15/2} transitions [8] (the horizontal axis shows transition energy in cm⁻¹ on all panels, while the vertical axis shows the measured photoluminescence intensity in arbitrary units on the bottom panel, and the calculated oscillator strength in 10⁻⁸ atomic units on the top and middle panels)

to the value of 39.72 in order to reproduce the experimental value for $^4I_{13/2}$ – $^4I_{15/2}$ splitting [27, 28]. The crystalline environment of Er^{3+} ion at the non-centrosymmetric C_2 site of the crystal structure of yttrium sesquioxide was represented by six nearest oxygen ions, approximated by negative $2e$ point charges dressed with the ECP of a Ne atom. The atomic coordinates were taken from synchrotron diffraction data on Y_2O_3 [29]. The C_2 site is related to a cubic coordination polyhedron with two oxygen ions removed along the face diagonal of the cube. However, since a Si nanocluster is too large for an *ab initio* treatment, its effect was modeled by a single highly polarizable Be atom, placed on the axis of symmetry. The Be atom was also described with the SBKJC basis set and ECP. To prevent the artificial charge transfer between the Er^{3+} ion and Be atom, Be was surrounded by four oxygen ions as well.

The wavefunctions of the ground and excited states of the model system were built following the protocol due to Koseki, Fedorov *et al.* [24]. First, the state-averaged (SA) multi-configurational self-consistent field method (MCSCF) was employed to optimize the orbitals of the quadruplet. The complete active space consisted of configuration state functions (CSF) obtained by all possible distribution of the 11 electrons over the seven $4f$ -orbitals. The incorporation of the $5s, 5p$ -orbitals into the active space in some preliminary calculations was found to have negligible effect on both the level splitting and transition dipole moments between the $^4I_{13/2}$ and $^4I_{15/2}$ sublevels. All 13 quadruplet states that originate from the 4I term of the Er^{3+} ion were used in the state-averaging procedure. On the second step, the 11 lowest doublet states that arises from 2H term of the Er^{3+} ion were added, and the spin-orbit Hamiltonian matrix was constructed in the basis of 74 states, originating from all M_L components of 4I and 2H terms. The dipole transition moments were calculated between the mixed-spin states diagonalizing the spin-orbit Hamiltonian. The active space on the second step was extended then to include also the $2s, 2p$ -orbitals of Be atom in order to describe its polarization contribution to the different electronic states. In addition, first-order CI treatment

(FOCI) [30] was employed, where single excited configurations from the complete active space reference are added to the MCSCF wave function in order to account for the polarization of the Er^{3+} ion in different electronic states. The resulting wavefunction included 167,706 CSF for the doublet and 125,664 CSF for the quadruplet basis states.

Results and discussion

The calculation of the energy levels and transition dipole moments were carried out for two model systems that differ in their geometry. In both of these models, the Er atom was surrounded by six oxygen atoms (Fig. 2). The atomic coordinates correspond to the C_2 site in the Y_2O_3 crystal structure. In system I, we choose 5 Å separation between Er and Be, modeling the close proximity between Er and Si with no direct bonding. System II, in contrast, modeled the Er^{3+} ion placed far away from the Si nanocluster with 50 Å separation between Er and Be. In this latter system, the Be orbitals were excluded from MCSCF active space. In both cases the effective nuclear charge for Er^{3+} was fixed at the value of $Z_{\text{eff}}=39.72$ as determined from atomic calculations within the same basis set. This value is close to the actual nuclear charge (+68) minus the number of electrons that are treated implicitly by ECP (46 electrons in total). The difference is due to the nodeless structure of $4f$ orbital, when ECPs are employed. The relative energies of the lowest 15 states (forming degenerate pairs due to C_2 site symmetry) are reported in Table 1. The energy levels for both systems I and II are close to each other and reproduce experimental data reasonably well.

The calculated transition dipole moments are plotted on Fig. 3. The experimental absorption spectra are also shown for comparison. One can see from this Figure, that when the polarizable Be atom is far away from the Er^{3+} ion, the spectral profile reproduces the experimental spectrum well, while in the proximity of Be the profile changes its shape, and the emission intensity increases by a factor of three.

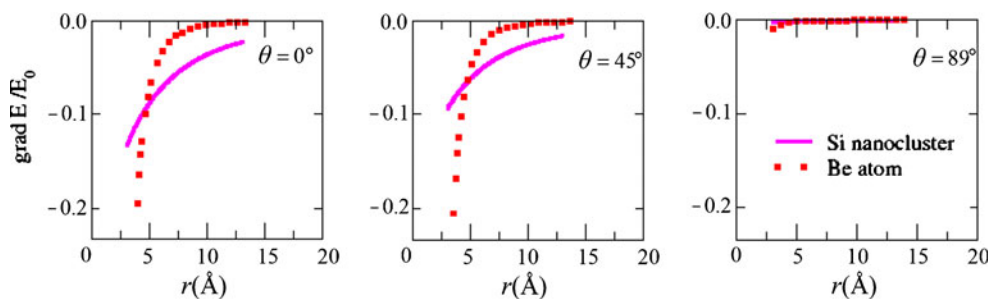


Fig. 4 The gradient of the electric field produced by a Be atom (dotted line) and a Si nanocluster of 15 Å radius (solid line) as a function of the distance r to the surface of each particle. Calculations were performed in the dipole frame using Eq. 1 and empirical values

for the polarizability of a Be atom in vacuum (9.3 \AA^3) and 15 Å Si nanocluster ($2.824 \cdot 10^3 \text{ \AA}^3$). The electric fields are taken relative to the external electric field E_0 and are shown for the three (fixed) polar angles of 0° (left panel), 45° (middle panel), and 89° (right panel)

Next we extrapolated the results of our *ab initio* calculations to the presence of a silicon nanocluster with a realistic size of approximately 15 Å. For this purpose, we used the classical electrodynamic equation

$$\nabla E(r)/E_0 = -5\alpha \cos\theta/r^4. \quad (1)$$

Here ∇E is the gradient of the electric field generated by the polarizable sphere shown on Fig. 1, α is polarizability of this sphere, r is the distance to the center of this sphere, and θ is the angle, formed by the external field of the strength E_o and the normal direction to the surface of the sphere. The gradients of the electric field produced by the Be atom and Si nanocluster of 15 Å radius in three different directions are plotted on Fig. 4. For the fair comparison, Si nanoclusters results are presented as a function of the distance r to the surface (defined as the distance to the center less the nanoparticle radius). In the computations, we used the empirical values for the polarizability of the Be atom in vacuum (9.3 \AA^3) and 15 nm Si nanocluster ($2.824 \cdot 10^3 \text{ \AA}^3$).

One can see from Fig. 4 that the electric field gradient produced by the Si nanoparticle at the range of distances 3–10 Å from its surface is within 50% of numerical values produced by Be atom at the distance of 5 Å. This conclusion is valid for a wide range of angles θ . It is the gradient of the electric field that polarizes the f -states, removing the center of symmetry for Er^{+3} cation. Thus gradient of the electric field generates the oscillator strength of $f-f$ transitions that would vanish in an entirely centro-symmetric environment. Therefore, the effect of the silicon nanocluster is expected to be similar to the emission enhancement due to the proximity of the Be atom as predicted in this work.

Conclusions

The possibility of enhanced emission from Er^{+3} ions embedded in the glass matrix and in the presence of silicon nanoclusters is investigated from first principles by using a model system that help simulate the polarization effects in the Er doped material. The mechanism of a local field concentration due to dielectric permeability of the Si nanoparticle, that is different from a silica matrix, is found to be feasible. Here, we report a factor of three increase in the $f-f$ transition probability in Er^{+3} ions due to the proximity of a polarizable Be atom. The classical extrapolation to the silicon nanocluster of 15 Å radius predicts an effect of similar magnitude under realistic conditions of silicon doped silica matrix.

Acknowledgments This work is supported in part by the UCF Nanoscience Technology Center and the Gesellschaft für Schwerionenforschung. The authors would like to thank Prof. Ehresmann, Dr. Demekhin,

Dr. Fedorov for discussions, E. Vinogradova for help with the manuscript preparation, and the UCF Institute for Simulation and Training (IST) Stokes HPCC facility for generous donation of the computer time.

References

- Lin H et al (2003) Er^{+3} doped $\text{Na}_2\text{O}-\text{Nb}_2\text{O}_5-\text{TeO}_2$ glasses for optical waveguide laser and amplifier. *J Phys D Appl Phys* 36:812–817
- Seat HC, Sharp JH (2003) $\text{Er}^{+3}/\text{Yb}^{+3}$ -codoped Al_2O_3 crystal fibres for high-temperature sensing. *Meas Sci Technol* 14:279–285
- Lira A et al (2004) Spectroscopic characterization of Er^{+3} transitions in $\text{Bi}_4\text{Si}_3\text{O}_{12}$. *J Phys Condens Matter* 16:5925–5936
- Daldo N et al (2005) Absorption cross section and signal enhancement in Er-doped Si nanocluster rib-loaded waveguides. *Appl Phys Lett* 86:261103
- Maurizio C et al. (2006) Er site in Er-implanted Si nanoclusters embedded in SiO_2 . *Phys Rev B* 74:205428
- Serincan U et al (2007) Variation of photoluminescence from Si nanostructures in SiO_2 matrix with Si^{+} post implantation. *Nucl Instrum Methods Phys Res B Beam Interact Mater Atoms* 254:87–92
- Kik PG, Polman A (2001) Exciton-erbium energy transfer in si nanocrystal-doped SiO_2 . *Mater Sci Eng B Solid-State Mater Adv Technol* 81:3–8
- Franzo G, et al (2000) Er^{+3} ions-Si nanocrystals interactions and their effects on the luminescence properties. *Appl Phys Lett* 76:2167–2169; Dammak M, Maalej R, Kamoun M, Deschanvres JL (2003) Crystal field analysis of erbium doped yttrium oxide thin films in C_2 and C_{3i} sites. *Phys Stat Solid B-Basic Res* 239:193–202
- Kik PG, Polman A (2001) Gain limiting processes in Er-doped Si nanocrystal waveguides in SiO_2 . *J Appl Phys* 91:534–536
- Han HS et al (2002) Coefficient determination related to optical gain in erbium-doped silicon-rich silicon oxide waveguide amplifier. *Appl Phys Lett* 81:3720–3722
- Clement TJ et al (2006) Nanocluster sensitized erbium-doped silicon monoxide waveguides. *Opt Express* 14:12151–12162
- Mertens H et al (2005) Absence of the enhanced intra-4f transition cross section at 1.5 μm of Er^{+3} in Si-rich SiO_2 . *Appl Phys Lett* 86:241109
- Prakash GV et al. (2001) Structural and optical properties of silicon nanocrystals grown by plasma-enhanced chemical vapor deposition. *J Nanosci Nanotech* 1:159–168
- Klimov VV, Ducloy M, Letokhov VS (2001) Spontaneous emission of an atom in the presence of nanobodies. *Quantum Electron* 31:569–586
- Judd BR (1962) Optical absorption intensities of rare-earth ions. *Phys Rev* 127:750
- Smentek L, Wybourne BG, Hess BA (2001) Judd-Olfelt theory in a new light on its (almost) 40th anniversary. *J Alloys Compd* 323:645–648
- Matsuoka O (1992) Relativistic self-consistent-field methods for molecules. 3. All-electron calculations on diatomics HI , HI^+ , AtH , and AtH^+ . *J Chem Phys* 97:2271–2275
- Dyall KG (1993) Relativistic effects on the bonding and properties of the hydrides of platinum. *J Chem Phys* 98:9678–9686
- Sanoyama E, Kobayashi H, Yabushita S (1998) Spin-orbit CI study on multiplet terms of trivalent lanthanide cations. *J Mol Struct Theochem* 451:189–204
- Dyall KG (1994) 2nd-order moller-plesset perturbation-theory for molecular Dirac-Hartree-Fock wave-functions - theory for up to 2 open-shell electrons. *Chem Phys Lett* 224:186–194
- Visscher L, Lee TJ, Dyall KG (1996) Formulation and implementation of a relativistic unrestricted coupled-cluster method including noniterative connected triples. *J Chem Phys* 105:8769–8776

22. Fedorov D, Schmidt MW, Koseki S, Gordon S (2004) Spin-orbit coupling and applications to chemistry, recent advances in relativistic molecular theory. *World Scientific* 5:107–136
23. Koseki S, Schmidt MW, Gordon MS (1998) Effective nuclear charges for the first- through third-row transition metal elements in spin-orbit calculations. *J Phys Chem A* 102:10430–10435
24. Koseki S et al (2001) Spin-orbit splittings in the third-row transition elements: Comparison of effective nuclear charge and full Breit-Pauli calculations. *J Phys Chem A* 105:8262–8268
25. Cundari TR, Stevens WJ (1993) Effective core potential methods for the Lanthanides. *J Chem Phys* 98:5555–5565
26. Cao XY, Dolg M (2002) Segmented contraction scheme for small-core lanthanide pseudopotential basis sets. *J Mol Struct Theochem* 581:139–147
27. Sugar J, Reader J (1973) Ionization energies of doubly and triply ionized rare-earths. *J Chem Phys* 59:2083–2089
28. Kelleher DE et al (1999) The new NIST atomic spectra database. *Phys Scr* T83:158–161
29. Maslen EN, Streletsov VA, Ishizawa N (1996) A synchrotron X-ray study of the electron density in C-type rare earth oxides. *Acta Crystallogr B Struct Sci* 52:414–422
30. Lengsfeld BH et al (1981) On the use of corresponding orbitals in the calculation of non-orthogonal transition moments. *J Chem Phys* 74:6849–6856